Applied Catalysis B: Environmental 129 (2013) 482–490

Contents lists available at SciVerse ScienceDirect

Applied Catalysis B: Environmental

journal homepage: www.elsevier.com/locate/apcatb

$CdIn_2S_4$ microsphere as an efficient visible-light-driven photocatalyst for bacterial inactivation: Synthesis, characterizations and photocatalytic inactivation mechanisms

Wanjun Wang[a], Tsz Wai Ng[a], Wing Kei Ho[b,**], Jianhui Huang[b,c], Shijing Liang[d], Taicheng An[e], Guiying Li[e], Jimmy C. Yu[f], Po Keung Wong[a,*]

[a] School of Life Sciences, The Chinese University of Hong Kong, Shatin, N.T., Hong Kong, China
[b] Department of Science and Environmental Studies, The Hong Kong Institute of Education, Taipo, N.T., Hong Kong, China
[c] Department of Environmental and Life Sciences, Putian University, Putian 351100, China
[d] State Key Laboratory Breeding Base of Photocatalysis, Research Institute of Photocatalysis, Fuzhou University, Fuzhou 350002, China
[e] State Key Laboratory of Organic Geochemistry, Guangzhou Institute of Geochemistry, Chinese Academy of Sciences, Guangzhou 510640, China
[f] Department of Chemistry, The Chinese University of Hong Kong, Shatin, N.T., Hong Kong, China

ARTICLE INFO

Article history:
Received 17 July 2012
Received in revised form
25 September 2012
Accepted 29 September 2012
Available online 8 October 2012

Keywords:
Photocatalytic inactivation
$CdIn_2S_4$
Ultrasonic spray pyrolysis
Partition system
Hydrogen peroxide

ABSTRACT

New types of visible-light-driven photocatalysts with high activity for bacterial inactivation are needed to address the problems caused by outbreak of harmful microorganisms. In this study, cadmium indium sulfide ($CdIn_2S_4$) microsphere, which can be synthesized continuously by a facile ultrasonic spray pyrolysis method, was used as an efficient photocatalyst in inactivation of *Escherichia coli* K-12 under visible light (VL) irradiation for the first time. The as-prepared $CdIn_2S_4$ showed a micro-spherical morphology with diameter of 0.5–1.0 μm. It had an energy band gap of 2.02 eV and BET surface area of 34.8 m^2/g. It was found that bacterial cells could also be effectively inactivated inside a partition system without the direct contact with the photocatalyst, which was attributed to the diffusible photon-generated hydrogen peroxide (H_2O_2) rather than hydroxyl radicals (•OH). Large amounts of H_2O_2 were produced from both conduction and valance bands with the involvement of superoxide ($•O_2^-$). The used $CdIn_2S_4$ could be easily recycled by the partition system without loss of activity. The destruction process of bacterial cells was from the cell wall to the intracellular components as confirmed by TEM study. In addition, the $•O_2^-$ and •OH radicals were also detected in the $CdIn_2S_4$-VL system by ESR spin-trap with DMPO trapping technology.

1. Introduction

Photocatalysis has been introduced as one of the promising processes in the inactivation of bacterial cells in water since 1985 [1]. This finding creates a new avenue for water sterilization. In particular, TiO_2-mediated bacterial inactivation appears to be a more reliable technique compared to traditional bacterial inactivation methods such as chlorination and UV disinfection [2–5]. Chlorination may generate carcinogenic disinfection byproducts, while UV disinfection alone may not be effective for some UV-resistant bacteria. However, the use of TiO_2 in practical application is limited by its low utilization efficiency of solar energy because of the restricted absorption in UV region, which only accounts for 5% of the whole solar spectrum. Doped and composite TiO_2, including S-doped TiO_2 [6], Fe-doped TiO_2 [7], AgBr/TiO_2 [8] and Ag/AgBr/TiO_2 [9] have explored to improve the light absorption to visible light (VL) region. Meanwhile, many researchers have also turned their focus on the development of novel single-phase visible-light-driven (VLD) photocatalysts. However, the identified VLD photocatalysts for bacterial inactivation are rather limited [10,11]. It has been reported that multicomponent metal sulfides and oxysulfides show photocatalytic activity [12], which implies that the multicomponent metal sulfide could be a new class of photocatalyst for bacterial inactivation. Among them, cadmium indium sulfide has been found to degrade Methylene Blue (MB) [13], indicating that it may represent a new VLD photocatalyst for bacterial inactivation.

Cadmium indium sulfide ($CdIn_2S_4$) is a semiconductor chalcogenide that belongs to the AB_2X_4 family of ternary compounds. $CdIn_2S_4$ is attracting increasing attention because it is a VLD

* Corresponding author. Tel.: +852 3943 6383; fax: +852 2603 5767.
** Corresponding author. Tel.: +852 2948 8255; fax: +852 2948 7726.
E-mail addresses: keithho@ied.edu.hk (W.K. Ho), pkwong@cuhk.edu.hk (P.K. Wong).

0926-3373/$ – see front matter © 2012 Elsevier B.V. All rights reserved.
http://dx.doi.org/10.1016/j.apcatb.2012.09.054

photosensitive semiconductor that has potential application in solar cells [14,15], hydrogen evolution [12] and organic dyes, such as MB degradation [13]. Interestingly, the VLD photocatalytic bacterial inactivation in aqueous media by $CdIn_2S_4$ has never been reported. $CdIn_2S_4$ has previously been synthesized by hot-wall epitaxy (HWE) method that requires a high temperature, high vacuum, and a transportation agent such as iodine [15]. Recently, hydrothermal method has also been introduced to the fabrication of $CdIn_2S_4$, but it requires long reaction time (60 h) and surfactants such as polyethylene glycol (PEG) to control the morphology of final products, which is unfavorable for low-cost and large-scale production [12]. Ultrasonic spray pyrolysis (USP) is a method of producing particles, in which a misted stream of precursor solution is dried, precipitated, and decomposed in a tubular furnace reactor [16]. Particles produced by USP are relatively uniform in size and composition because of the microscale reaction within droplets. It has been employed in the preparation of fine particles of metal sulfide, such as MS (M = Zn, Cd, Cu) [17] and MoS_2 [18]. Recently, the ternary sulfides MIn_2S_4 (M = Cd, Zn) and $AgIn_5S_8$ were also prepared by USP method for photocatalytic removal of NO in air [19].

Many reactive oxidative species, including hydroxyl radical (•OH), superoxide ($•O_2^-$) and hydrogen peroxide (H_2O_2), are involved in the UV-irradiated TiO_2 photocatalysis system. However, the fundamental mechanism underlying the VLD photocatalytic bacterial inactivation process has not been well-established. It is known that for an effective photocatalytic dye degradation process, the direct contact between pollutants and photocatalysts is important [20]. However, for the destruction of microorganisms, MS-2 phage can be inactivated mainly by the free •OH in the bulk solution without direct contact with the photocatalysts [21]. The inactivation of *Escherichia coli* K-12 has also been observed inside a semi-permeable membrane system (i.e. a partition system), which is ascribed to the function of photon-generated H_2O_2 acting as the disinfection agent [22,23]. These studies indicate that the VLD photocatalytic bacterial inactivation can take place without direct contact with the photocatalysts. Herein, we have synthesized nanocrystalline $CdIn_2S_4$ with micro-spherical morphology via USP method. The photocatalytic bacterial inactivation behaviors of the as-prepared $CdIn_2S_4$ under VL irradiation were investigated for the first time. To study the mechanism, chemical scavengers were used to interact with different reactive species in the VLD photocatalytic inactivation process. Moreover, a simple partition system with a semi-permeable membrane [20,22] to separate the photocatalyst from bacterial cells was employed to determine whether a direct contact between the photocatalyst and bacterial cell is required for the inactivation.

2. Experimental

2.1. Synthesis

The $CdIn_2S_4$ photocatalyst was prepared by a modified USP method [19] using $Cd(CH_3COO)_2{\cdot}2H_2O$, $InCl_3{\cdot}4H_2O$ and thiourea as the starting materials, which were purchased from Sigma Chemical Co. (USA) and used without further purification. A scheme for the USP synthesis apparatus was shown in Figure S1. In a typical process, 2 mmol $Cd(CH_3COO)_2{\cdot}2H_2O$, 4 mmol $InCl_3{\cdot}4H_2O$, and 10 mmol thiourea were added to 150 mL distilled water. A clear solution was obtained after vigorous stirring for 20 min. The solution was nebulized at 1.7 MHz ± 10% by an ultrasonic nebulizer (YUYUE 402AI, Shanghai) and then carried by air with flow rate of 10 L/min through a quartz tube surrounded by a furnace thermostated at 600 °C. The quartz reaction tube with the diameter of 3.5 cm had a long-length of 1 m. The products were collected in a percolator with distilled water, and then separated by centrifugation. After washed thoroughly with ethanol and distilled water, the products were finally dried under vacuum at 100 °C for 1 h.

For scavenging study, potassium dichromate [$K_2Cr_2O_7$ (Cr(VI)], sodium oxalate ($Na_2C_2O_4$) and isopropanol ($(CH_3)_2CHOH$) were purchased from Riedel–deHaën Chemical Co. (Germany). Ferric sulfate–ethylenediamine–tetraacetic acid [$FeSO_4$–EDTA (Fe(II)] was prepared by dissolving equal mole ratio of $FeSO_4{\cdot}7H_2O$ (AJAX Chemicals, Australia) and ethylenediamine–tetraacetic acid (EDTA, AJAX Chemicals, Australia) in distilled water. 4-Hydroxy-2,2,6,6-tetramethylpiperidinyloxy (TEMPOL) were obtained from Sigma Chemical Co. (USA). All of the chemicals were of analytical reagent grade and isopropanol was of HPLC grade and dehydrated.

2.2. Characterizations

X-ray diffraction (XRD) patterns were collected on a Bruker D8 Advance X-ray diffractometer with Cu Kα radiation. The accelerating voltage and the applied current were 40 kV and 40 mA, respectively. Data were recorded at a 2θ scan rate of $0.02^\circ\ s^{-1}$ in the 2θ range of 10° to 70°. The morphology of the products was examined by scanning electron microscopy (SEM, LEO, 1450VP) and transmission electron microscopy (TEM, FEI Tecnai G2 Spirit). UV–visible diffuse reflectance spectra (UV–vis DRS) of the powders were obtained for the dry-pressed disk samples using a Varian Cary 500 UV–vis spectrophotometer equipped with a labsphere diffuse reflectance accessory. $BaSO_4$ was used as a reflectance standard in the UV–vis DRS experiment. The specific surface area and porosity of the sample were measured by N_2 adsorption at 77 K on a Micrometritics ASAP2020 analyzer and calculated by the Brunauer–Emmett–Teller (BET) method.

The formation of $•O_2^-$ and •OH were detected by electron spin resonance (ESR) technology. ESR signals of spin-trapped paramagnetic species with 5,5-dimethyl-1-pyrroline N-oxide (DMPO) were recorded with a Brucker A300 spectrometer. As $•O_2^-$ was very unstable in water and slow reaction with DMPO, the involvement of $•O_2^-$ was examined in methanol. Catalase (CAT) activity determination was conducted using the Catalase Assay Kit (Cayman Chemical Company, Ann Arbor, MI, USA), following the protocol recommended by the manufacturer. One unit of CAT activity (nmol/min/mL) was defined as the amount of enzyme that would cause the formation of 1.0 nmol of formaldehyde per minute at 25 °C. Hydrogen peroxide (H_2O_2) was analyzed colorometrically by the POD (horseradish peroxidase)-catalyzed oxidation product of DPD (N,N-diethyl-*p*-phenylenediamine) at 551 nm [24]. DPD readily reacted with H_2O_2 to produce the radical cation, $•DPD^+$, which was stabilized by resonance and formed a fairly stable color, with one absorption maxima at 510 nm and one at 551 nm (maximum wavelength). By monitoring the absorption intensity at 551 nm, the concentration of H_2O_2 can be determined.

The morphology of bacterial cells before and after photocatalytic inactivation was examined by transmission electron microscopy (TEM, JEM-1200). After bacterial fixation, ultra-thin sections of 70 nm were made and examined, following the standard procedures described in our previous report [11,23]. To investigate the Cd^{2+} eluted from photocatalyst and the K^+ leakage from bacterial cells during the photocatalytic inactivation process, the mixture before and after inactivation treatment was collected and filtered through a Millipore filter (pore size of 0.45 μm). After filtration, the Cd^{2+} and K^+ concentration in the resulting clear solution were measured by a polarized Zeeman atomic absorption spectrophotometer (AAS) (Hitachi Z-2300, Japan).

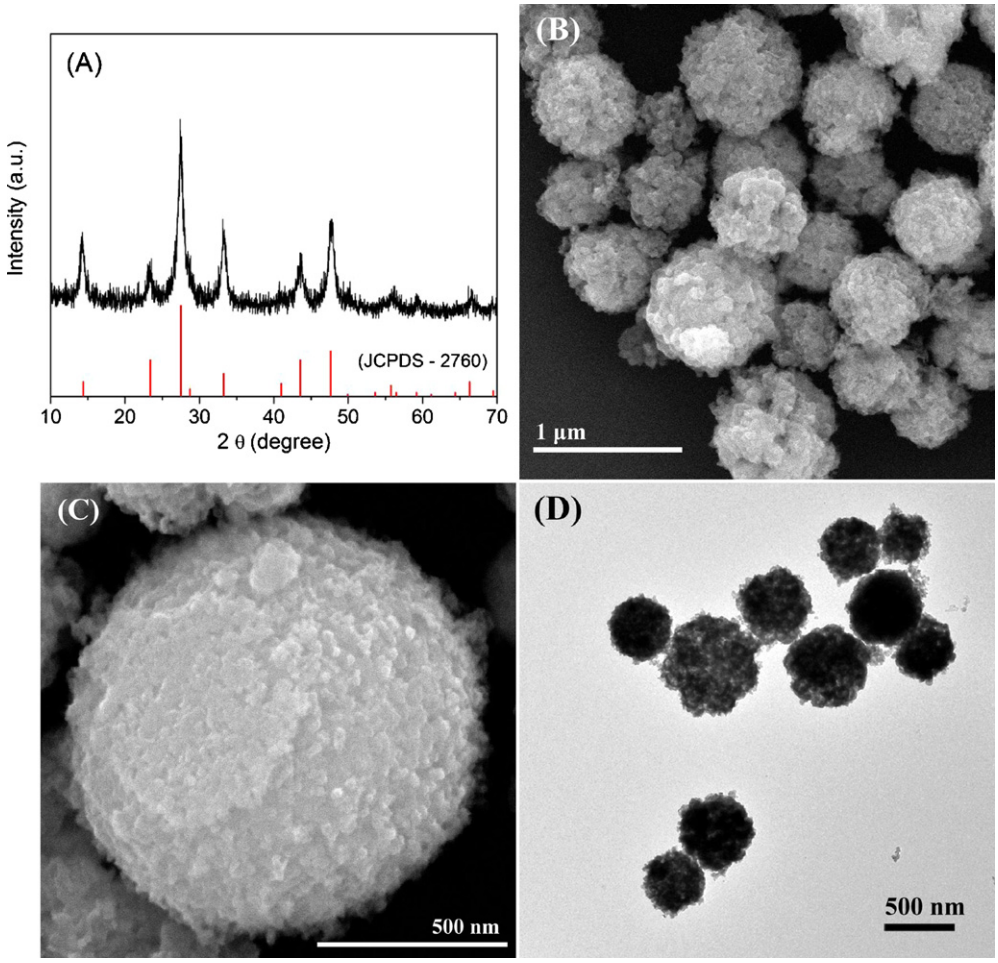

Fig. 1. (A) X-ray diffraction (XRD) pattern, (B and C) SEM images and (D) TEM image of $CdIn_2S_4$ microspheres synthesized by ultrasonic spray pyrolysis (USP) method at calcination temperature of 600 °C.

2.3. Photocatalytic bacterial inactivation

The VLD photocatalytic inactivation of *E. coli* K-12 was conducted using a 300 W Xenon lamp (Beijing Perfect Light Co. Ltd., Beijing) with a UV cutoff filter ($\lambda < 400$ nm) as light source. The VL intensity was measured by a light meter (LI-COR, USA) and the light intensity for the experiments was fixed at 193 mW/cm^2. No significant UV light was found (UVA = 0 mW/cm^2, UVB = 0.37 mW/cm^2, UVC = 0.0046 mW/cm^2). All glass apparatuses used in the experiments were autoclaved at 121 °C for 20 min to ensure sterility. The bacterial cells were cultured in nutrient broth (Lancashire, UK) at 37 °C and agitated at 200 rpm for 16 h. The cultures were then washed twice with sterilized saline (0.9% NaCl) solution by centrifugation for 5 min and then the cell pellet was re-suspended in sterilized saline solution. The photocatalyst and the saline suspension of washed cell were then added into a flask with an aluminum cover. The final cell density was adjusted to about 2×10^7 cfu (colony forming unit)/mL. The reaction temperature was maintained at 25 °C and the reaction mixture was stirred with a magnetic stirrer throughout the experiment. At different time intervals, aliquots of the sample were collected and serially diluted with sterilized saline solution. 0.1 mL of the diluted sample were then immediately spread on nutrient agar (Lancashire, UK) plates and incubated at 37 °C for 24 h to determine the number of viable cells (in cfu). Before irradiation, the suspensions were magnetically stirred in dark for 60 min to ensure the establishment of an adsorption/desorption equilibrium between the photocatalyst and bacterial cells. For comparison, three control experiments were conducted along with treatment experiments. The dark control was carried out with $CdIn_2S_4$ alone in dark, light control in the absence of $CdIn_2S_4$ under VL irradiation, and negative control without $CdIn_2S_4$ or VL irradiation. All the treatment and control experiments were performed in triplicates.

The setup of the partition system for this experiment is shown in Figure S2. The semi-permeable membrane used in the study was regenerate cellulose (RC) membrane purchased from Spectrum® Laboratories, Inc. (USA). The membrane thickness was about 25–50 μm. Twenty mL of *E. coli* K-12 saline suspension (2×10^7 cfu/mL) was pipetted into the semi-permeable membrane tube and the outside of the membrane was 50 mL of the $CdIn_2S_4$ saline suspension (100 mg/L), which was stirred continuously to keep the $CdIn_2S_4$ evenly distributed in the solution outside of the membrane. At different time intervals, aliquots of the cells inside the membrane tube were sampled and immediately diluted to determine the number of viable cells.

3. Results and discussion

3.1. Characterizations of photocatalyst

Fig. 1(A) shows the typical XRD pattern of the as-prepared $CdIn_2S_4$. It was clear that the powder diffraction pattern could be readily indexed to the pure phase of cubic $CdIn_2S_4$ (JCPDS No. 27-60, space group: Fd−3m). No other impurities, such as binary sulfides,

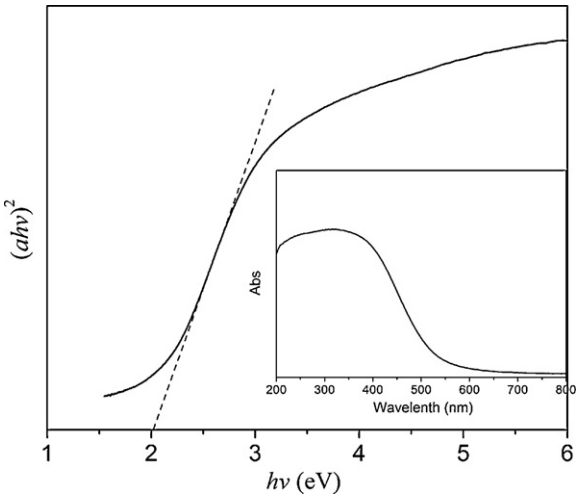

Fig. 2. Plots of the $(\alpha h\upsilon)^2$ vs the absorbed energy $(h\upsilon)$ and UV–vis diffuse reflectance spectra (inset) of the as-prepared $CdIn_2S_4$ microspheres.

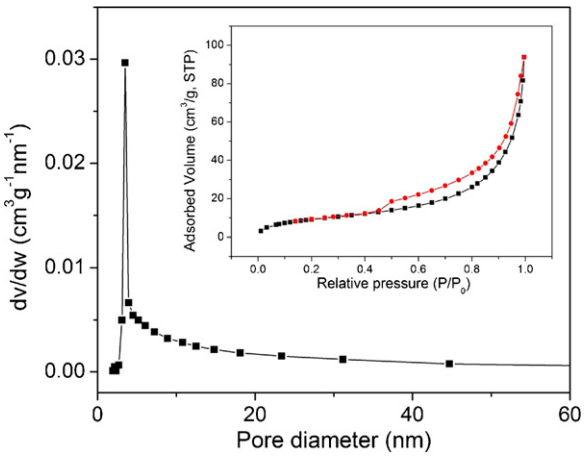

Fig. 3. Nitrogen adsorption–desorption isotherms (inset) and the Barret–Joyner–Halenda (BJH) pore size distribution plot of the as-prepared $CdIn_2S_4$ microspheres.

oxides or organic compounds related to reactants were detected. The average crystallite size calculated from the Scherrer equation was about 10.8 nm, indicating nanocrystalline nature of the as-prepared $CdIn_2S_4$. SEM and TEM images clearly showed that the $CdIn_2S_4$ particles have microsphere morphologies with diameters of about 0.5–1.0 μm, which were assembled by numerous small nanocrystallites (Fig. 1). Because the USP method was a representative droplet-to-particle conversion process, in which the precursor solution was first nebulized to produce aerosol. The droplet in the aerosol had similar function as micro-reactor, thus reaction was completed within each droplet, resulting in precisely microspherical structure. On the other hand, thiourea formed complexes with Cd^{2+} and In^{3+} in aqueous solutions. These thiourea complexes could be thermally decomposed to form metal sulphides, leading to the high purity of $CdIn_2S_4$ while avoiding the use of high temperature, high pressure, and long reaction time. The high quality products can be generated continuously at a rate of several grams per hour without intermission, which is easy to be amplified as practical industry production with large-scale.

The optical absorption of the as-prepared samples was measured by diffuse reflectance spectroscopy. As shown in Fig. 2, the absorption cutoff wavelength of the as-prepared $CdIn_2S_4$ microsphere was about 520 nm, suggesting that the present material may be VL-responsive. Meanwhile, the steep absorption edge and strong absorption in the VL region revealed that the absorption band of $CdIn_2S_4$ was caused by the transition of photon-generated e^- from the valence band (VB) to the conduction band (CB) instead of the transition from the metal impurity levels [25]. The energy band gap (E_g) of semiconductor could be estimated by using the expression $\alpha h\upsilon = A(h\upsilon - E_g)^n$ [26], where α was the absorption coefficient, $h\upsilon$ was the photon energy, and $n = 1/2$ for $CdIn_2S_4$ as a direct transition semiconductor [27]. The E_g was measured with the help of absorption spectra and a graph of $(\alpha h\upsilon)^2$ vs $h\upsilon$ was plotted (Fig. 2). The extrapolation of the straight line to $(\alpha h\upsilon)^2 = 0$ gave the value of E_g to be about 2.02 eV, which was expected to be active under VL region. For the band structure, the top of the VB comprised predominantly S 3p, while the CB comprised the In 5s and 5p states with some contribution of Cd 5s and 5p states [12].

The N_2 adsorption–desorption isotherms and pore size distribution curve of the resulting sample was shown in Fig. 3. The pore size distribution was calculated from the desorption branch of nitrogen isotherms by Barret–Joyner–Halenda (BJH) method using the Halsey equation [28]. In Fig. 3, the physioadsorption isotherms could be classified as type IV with hysteresis loops according to the IUPAC classification [29], indicating the mesoporous nature of the as-prepared sample. A broad pore size distribution was observed with average pore size of about 11.9 nm. The BET specific surface area and pore volume were estimated to be 34.8 m^2/g and 0.15 cm^3/g, respectively. This porosity could be attributed to the contribution of interparticle pores. It has been reported that the present microsphere structure with mesopores can serve as efficient transport paths for reactants and products in photocatalytic reactions [30,31]. In addition, the large surface areas of $CdIn_2S_4$ microsphere structure not only provides more active sites for the bacterial inactivation with direct contact to the photocatalyst surface, but also effectively promotes the intrinsic separation of the electron-hole pairs when without the direct contact with photocatalysts [32,33]. The high surface area and porous structure resulting from spherical morphology also indicates the enhanced light harvesting due to multiple scattering [34,35] and the increased photocatalytic oxidation activity [36].

3.2. Photocatalytic bacterial inactivation

E. coli K-12, a common waterborne microorganism, was chosen as a representative microorganism to evaluate the photocatalytic inactivation performances of $CdIn_2S_4$. In the dark, light and negative control experiments, the bacterial population remained unchanged even after 3 h, indicating no toxic effect of $CdIn_2S_4$ to *E. coli* K-12 cells and no photolysis of bacterial cells under VL irradiation alone. However, with VL irradiation, the as-prepared 50 mg/L $CdIn_2S_4$ exhibited photocatalytic activity for the inactivation of *E. coli* K-12 (Fig. 4). The inactivation efficiency was further improved with the increase of photocatalyst concentration, and total inactivation of about 7 log of bacterial cells was achieved after 3 h of irradiation in the presence of 100 mg/L $CdIn_2S_4$. When further increasing the photocatalyst concentration to 200 mg/L, the photocatalytic inactivation efficiency was slightly improved. Therefore, from both a cost-saving and an environmental point of view, 100 mg/L was chosen as the optimal concentration and used in all the following experiments.

Bacterial regrowth test was conducted to evaluate the effectiveness of photocatalytic bacterial inactivation by $CdIn_2S_4$. After the completed photocatalytic inactivation treatments for 3 h, the reaction mixture was sampled and underwent a 96 h recovery period to determine the bacterial regrowth. Results (data not shown) indicated that no detectable bacterial count (in cfu/mL) was observed after 96 h dark incubation period. It suggests that 3 h is an effective disinfection time (EDT) for VLD photocatalytic inactivation of

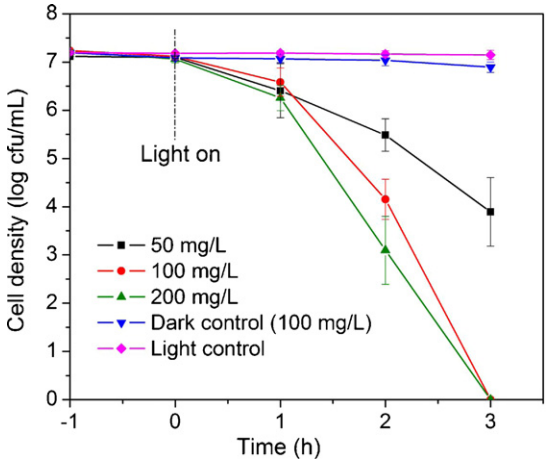

Fig. 4. Photocatalytic inactivation efficiency against *E. coli* K-12 (2×10^7 cfu/mL, 50 mL) in the presence of $CdIn_2S_4$ (100 mg/L) under VL irradiation.

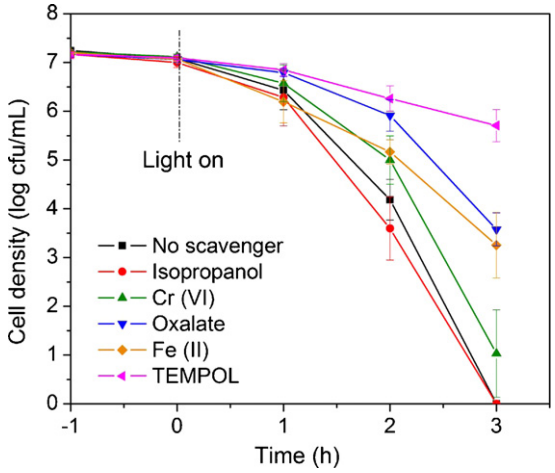

Fig. 5. Photocatalytic inactivation efficiency against *E. coli* K-12 (2×10^7 cfu/mL, 50 mL) with different scavengers (0.05 mmol/L Cr(VI), 0.5 mmol/L isopropanol, 0.5 mmol/L sodium oxalate, 0.1 mmol/L Fe(II)-EDTA, 2 mmol/L TEMPOL) in the presence of $CdIn_2S_4$ (100 mg/L) under VL irradiation. No bacterial inactivation occurs in the dark and light controls.

E. coli K-12 by $CdIn_2S_4$, which is defined as the time required for complete bacterial inactivation without regrowth in a subsequent dark period for 96 h [37]. This result also suggests that photocatalytic inactivation by $CdIn_2S_4$ lead to irreversible damage to *E. coli* K-12. Furthermore, to eliminate the possibility that the inactivation of bacterial cells might be resulted from Cd^{2+} elution, the concentration of Cd^{2+} was monitored during the inactivation process (Figure S4). Results showed that less than 0.2 mg/L Cd^{2+} was eluted after 3 h of VL irradiation, and the addition of 0.2 mg/L Cd^{2+} would not cause any bacterial inactivation (Figure S5), indicating that the bacterial cells were photocatalytically inactivated by $CdIn_2S_4$ instead of eluted toxic ions. This result also indicated that only less than 0.8 wt.% of photocatalyst was possibly photo-corroded after disinfection treatment, exhibiting high photo-stability.

3.3. Role of different reactive species

As mentioned above, the h^+, $^\bullet OH$, H_2O_2 and $^\bullet O_2^-$ are often proposed to be the reactive oxidative species responsible for the photocatalytic bacterial inactivation. However, which one of them plays the most important role in the photocatalytic reaction process is still unclear, and is quite different from various photocatalytic systems. To investigate the exact roles of these reactive oxidative species in the inactivation process, we performed the scavenging study, which employing different scavengers individually to remove the specific reactive species, so that we can understand the function of different reactive species in this photocatalytic inactivation process based on the change of inactivation efficiency. The scavengers used in this study were sodium oxalate for h^+ [38,39], isopropanol for $^\bullet OH$ [40,41], Cr(VI) for e^- [40,42], Fe(II) for H_2O_2 [23,39], and TEMPOL for $^\bullet O_2^-$ [43]. Before conducting the experiment, the applied concentrations of each scavenger were optimized to show their significant scavenging effect but would not cause toxicity to the bacterial cells [22]. The pH of the reaction mixture without scavengers was maintained at 6.85 and would only change from 6.42 to 7.15 after adding the tiny concentration of these scavengers, so that the pH effect on the photocatalytic inactivation efficiency could be negligible in the scavenging study [22], which is also supported by previous report that no significant photocatalytic inactivation efficiency of *E. coli* by TiO_2 was observed when the pH was changed from 5.6 to 8.1 [44]. In the present study, no significant bacterial inactivation was found in dark and light controls, further confirming the non-toxicity of these scavengers to the bacterial cells (Figure S3). As shown in Fig. 5, with the addition of isopropanol, the inactivation efficiency remained almost the same as no scavenger added, indicating the $^\bullet OH$ was not important in this VLD photocatalytic inactivation process. However, obvious inhibition effect of bacterial inactivation was observed when oxalate and Cr(VI) were used to quench h^+ and e^-, respectively. This confirms the important roles of h^+ and e^-, since other reactive oxidative species, such as $^\bullet O_2^-$ and H_2O_2, are produced from them. With the addition of Fe(II) to scavenge H_2O_2, the inactivation efficiency was greatly decreased, indicating H_2O_2 plays a major role in the photocatalytic inactivation in this system, which matches well with our previous studies [22,23]. The addition of TEMPOL was also found to greatly inhibit the inactivation process, because in the conduction band (CB), the H_2O_2 could be produced from $^\bullet O_2^-$. The quenching of $^\bullet O_2^-$ would also decrease the amount of H_2O_2. On the other hand, it has also been reported that the $^\bullet O_2^-$ has direct inactivation effect on the bacterial cells [22], resulting in a more significant inhibition effect on the inactivation efficiency with the $^\bullet O_2^-$ scavenger.

3.4. Partition system and the role of H_2O_2

To further investigate the direct contact effect between photocatalyst and bacterial cell, and determine whether the photocatalytic inactivation occurs on the photocatalyst surface or in the bulk solution, we employed a partition system to separate bacterial cell from photocatalyst surface. The *E. coli* K-12 suspension was injected into the semi-permeable membrane tube and the $CdIn_2S_4$ was dispersed outside of the membrane tube. The *E. coli* K-12 with molecular weight of about 2.6×10^6 Da and the $CdIn_2S_4$ microsphere with a diameter of about 0.5–1.0 μm cannot pass through the membrane, so that the direct contact between bacterial cell and photocatalyst was prohibited. No bacterial inactivation was observed in dark and light control experiments (Figure S6). As shown in Fig. 6, the *E. coli* K-12 cells could also be effectively inactivated inside the membrane tube. About 7 log of bacterial cells were almost completely inactivated without the direct contact with the photocatalyst, indicating that the direct contact is not important for the VLD photocatalytic bacterial inactivation by $CdIn_2S_4$. Some reactive oxidative species can diffuse into the partition system and cause the bacterial inactivation. To study this mechanism, scavenging study was also performed inside the membrane tube. The addition of Fe(II) as H_2O_2 scavenger significantly inhibited the inactivation process and about 5.5 log of bacterial population was still observed inside the membrane tube after 3 h of VL irradiation, while the addition of isopropanol as $^\bullet OH$ scavenger had almost no

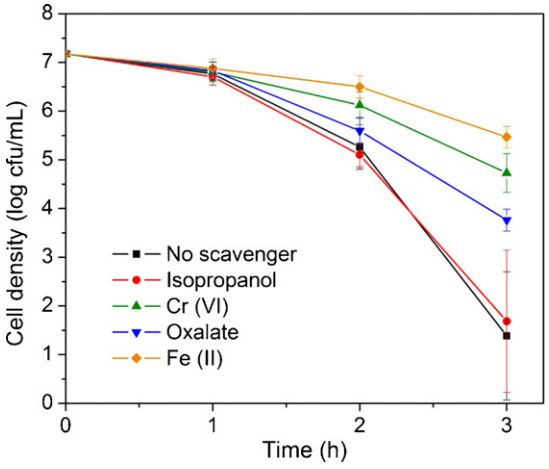

Fig. 6. Photocatalytic inactivation efficiency against *E. coli* K-12 (2×10^7 cfu/mL, 20 mL) in the inner compartment of the partition system. The outer compartment was the $CdIn_2S_4$ suspension (100 mg/L) with the addition of different scavengers (0.05 mmol/L Cr(VI), 0.5 mmol/L sodium oxalate, 0.1 mmol/L Fe(II)-EDTA) under VL irradiation.

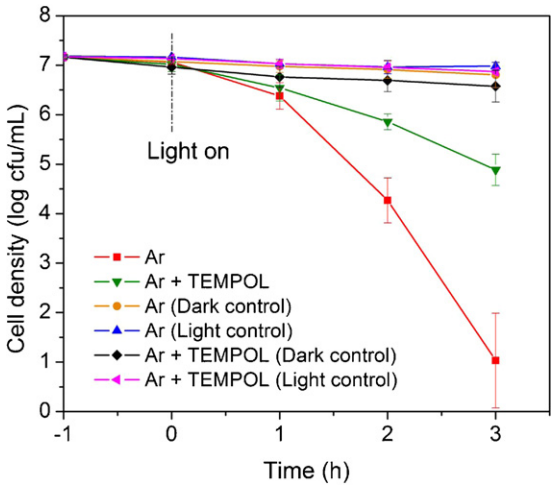

Fig. 8. Photocatalytic inactivation efficiency against *E. coli* K-12 (2×10^7 cfu/mL, 50 mL) by $CdIn_2S_4$ microspheres under anaerobic condition (argon aeration) with the addition of TEMPOL (2 mmol/L) under VL irradiation.

influence on the inactivation efficiency. This result indicates the diffusible reactive oxidative species that are responsible for the inactivation without direct contact seems to be H_2O_2, rather than traditionally regarded •OH. Because it is known that the life-span of •OH is extremely short, thus it is supposed to be quickly quenched in the aqueous media before it can cause any damage to the bacterial cells in the partition system. Actually, •OH will promptly combine with another •OH to produce H_2O_2 [45,46], which is highly responsible for the bacterial inactivation.

To further confirm the role of H_2O_2, we applied the DPD/POD method, which has been proved to be an effective method for low concentration of H_2O_2 [24], to directly monitor the production of H_2O_2. It was found that the production of H_2O_2 increased dramatically under VL irradiation (Fig. 7). After 0.5 h of irradiation, the concentration of H_2O_2 reached a constant value, due to the decomposition of H_2O_2 in parallel with its production [47,48]. The equilibrium concentration for H_2O_2 produced was estimated to be 61.7 μmol/L, which far exceeded the concentration of H_2O_2 produced in TiO_2-based system (0.1–1.0 μmol/L) [48], exhibiting great potential of $CdIn_2S_4$ to be used in H_2O_2-oriented VLD photocatalytic applications. It should be noted that direct addition of this concentration of H_2O_2 would not have significant bacterial inactivation efficiency, because the small concentration of H_2O_2 was generated continuously under VL irradiation and interacted with the bacterial cells in situ once it was produced [22]. So the decomposition of H_2O_2 would be minimized in the presence of bacterial cells, and the total accumulated concentration of H_2O_2 that interacted with bacterial cells far exceeded the equilibrium concentration detected, which is a significant advantage of using $CdIn_2S_4$-VL photocatalytic system instead of direct H_2O_2 disinfection, because mild concentration of H_2O_2 is continuously generated without external supplement of high concentration of H_2O_2 in traditional H_2O_2 disinfection methods.

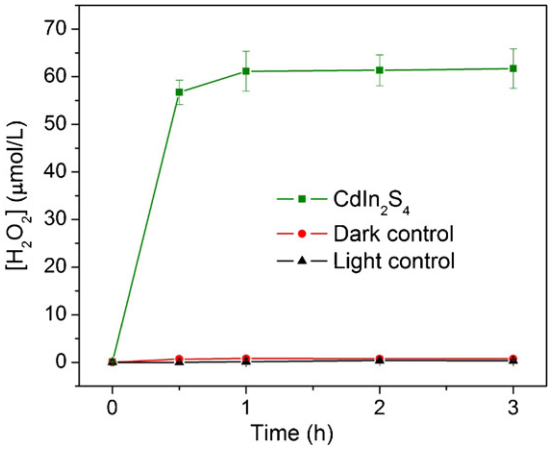

Fig. 7. Accumulation of H_2O_2 produced in the presence of $CdIn_2S_4$ microspheres (100 mg/L) under different VL irradiation time.

It is also found in Fig. 6 that, when interrupting H_2O_2 generation pathway from conduction band (CB) and valence band (VB) by Cr(VI) and oxalate, respectively, the inactivation efficiency in the partition system was decreased in both cases, indicating that H_2O_2 is produced from both CB and VB. In CB, H_2O_2 is believed to be produced by the reduction or disproportionation of $•O_2^-$, while in VB by the coupling of two •OH [45,46,49]. However, with argon (Ar) aeration to remove O_2 thus eliminating the $•O_2^-$ generation pathway from CB (*E. coli* is a kind of facultative anaerobe, and can live in anaerobic condition), the addition of TEMPOL as $•O_2^-$ scavenger also inhibited the inactivation efficiency (Fig. 8), indicating that $•O_2^-$ can also be produced from VB, and serve as another origin of H_2O_2 production, significantly promoting the overall H_2O_2 production in the present $CdIn_2S_4$ system. This result provides first experimental evidence for the previous reports that $•O_2^-$ formation may also occur as a result of h^+ trapping reactions in VB [50,51].

The stability and methods to recycle photocatalysts are extremely important for practical application. In this work, partition system was firstly used to easily recycle used photocatalysts, as the photocatalysts and the bacterial cells were already separated during disinfection treatment. The photocatalytic bacterial inactivation treatment was repeated five times with the same $CdIn_2S_4$ in partition system (Fig. 9). Results showed that no deterioration of inactivation efficiency was observed in the first four runs, further confirming the photo-stability of $CdIn_2S_4$. There was a slight decrease in inactivation efficiency in the fifth run, probably due to the contamination of photocatalyst surface, thus inhibiting the production of H_2O_2.

3.5. Bacterial catalase activity

Catalase (CAT) is a well-known antioxidant enzyme in bacterial cell that defends against oxidative stress from the environment. CAT catalyzes the conversion of H_2O_2 to oxygen and water, so a

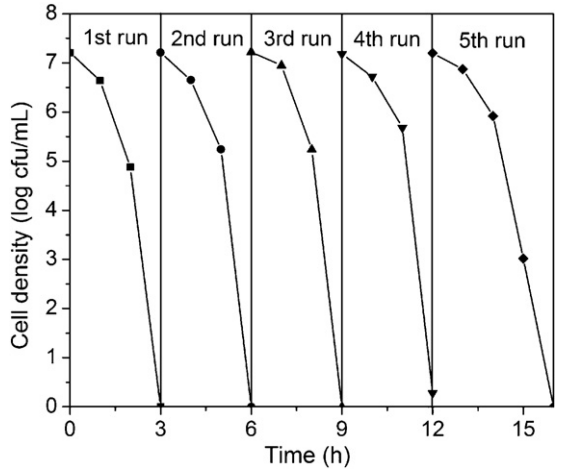

Fig. 9. Repeated experiments of photocatalytic inactivation of *E. coli* K-12 (2×10^7 cfu/mL, 50 mL) by $CdIn_2S_4$ microspheres under VL irradiation.

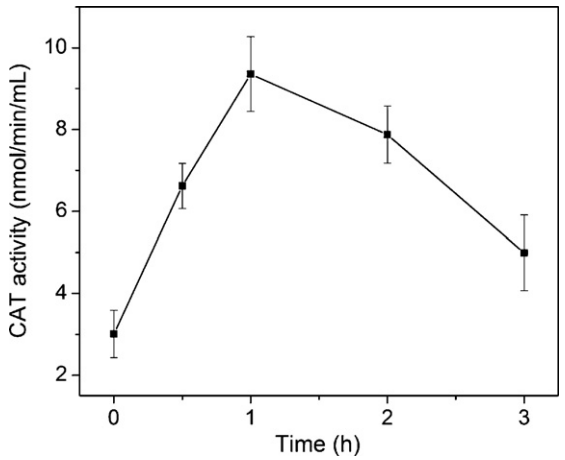

Fig. 10. Induction of CAT activity during photocatalytic inactivation of *E. coli* K-12 by $CdIn_2S_4$ under VL irradiation.

higher CAT activity indicates that bacterial cells are encountering a more significant H_2O_2 attack. Fig. 10 shows the induction of CAT activity during the photocatalytic inactivation process. It was found that the CAT level increased dramatically in the first 1 h, indicating large amounts of H_2O_2 were attacking bacterial cells at the beginning of inactivation process. This result matches well with the low photocatalytic inactivation efficiency in the first 1 h (Fig. 6), because the bacterial defense system induced high CAT level to protect the bacteria. After 1 h, the CAT activity decreased and the inactivation efficiency increased rapidly, indicating the amount of H_2O_2 produced by $CdIn_2S_4$ exceeded the protection ability of the defense system thus lead to the inactivation of bacterial cells. This result further provides indirect evidence that H_2O_2 plays an important role in the photocatalytic bacterial inactivation process.

3.6. Destruction process of bacterial cell

To understand the destruction process of bacterial cells by diffusing H_2O_2 in the $CdIn_2S_4$ photocatalytic system under VL irradiation, the structure and morphology of *E. coli* K-12 at the different stages of photocatalytic inactivation was examined by TEM studies (Fig. 11). Before the photocatalytic inactivation process, *E. coli* K-12 exhibited evenly rendered interior of the cell with a well-defined cell wall (Fig. 11A). After 3 h irradiation treatment (Fig. 11B), the central portion of the cell was still intact but part of the cell wall

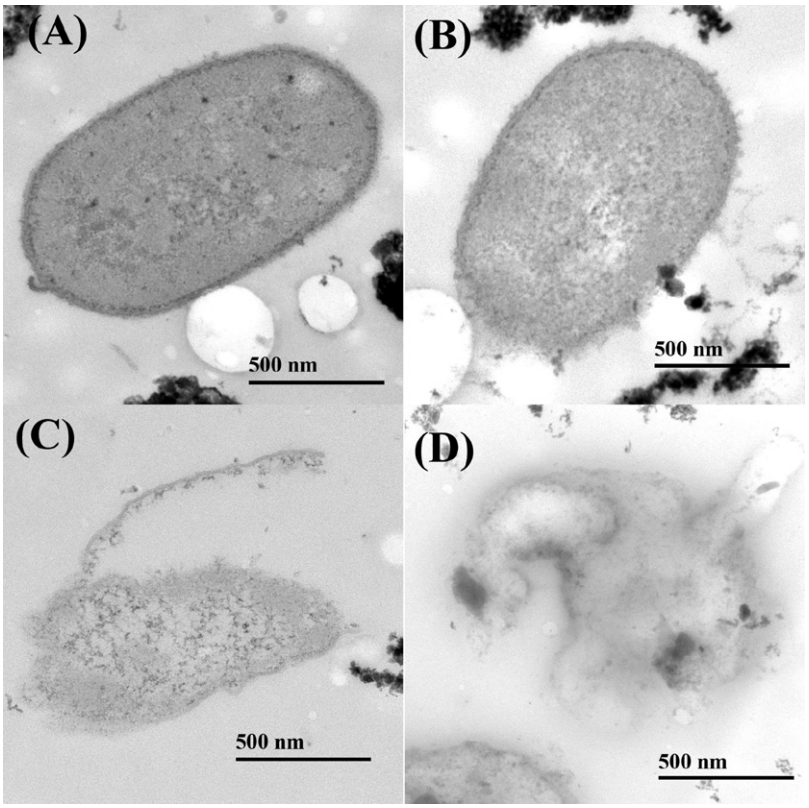

Fig. 11. TEM images of *E. coli* K-12 (2×10^7 cfu/mL, 50 mL) photocatalytically treated with $CdIn_2S_4$ microspheres (100 mg/L) under VL irradiation. (A) 0 h, (B) 3 h, (C) 6 h, and (D) 15 h.

structure appeared obscure, indicating initial damage to the cell wall and cytoplasmic membrane. Potassium ion (K^+), a component virtually existing in bacterial cells and involving in the regulation of polysome content and protein synthesis, quickly leaked from the bacterial cells during the inactivation process (Figure S7), because of the permeability change of membrane, resulting in the loss of cell viability [52]. In contrast, there was no significant leakage of K^+ occurred in the dark, light and negative control experiments (Figure S6). After 6 h VL irradiation (Fig. 11C), the damage of cell wall structure was clearly observed, however, some of the cytoplasmic components still remained, indicating that although H_2O_2 can departure cell membrane and oxidize lipids, it cannot degrade the total organic components inside the cell, because its oxidation power is not high enough as •OH which can degrade many kinds of organic compounds. With the prolonged irradiation time, the whole cell became more and more translucent, and finally was completely destructed after 15 h, leaving only a small portion of cell debris (Fig. 11D). These results confirm that the destruction process of bacterial cell is to begin from cell wall to other intracellular components.

3.7. Analysis of radical generation

In order to explore the radical generation in this photocatalytic system under VL irradiation and further confirm the bacterial inactivation mechanism, the ESR spin-trap with DMPO technique was carried out on illuminated $CdIn_2S_4$ microspheres. In the dark, no signals could be detected. Under VL irradiation, the six characteristic peaks of the DMPO–•O_2^- adducts were observed, further confirming the formation of •O_2^- during the VLD photocatalytic inactivation process (Fig. 12A). In addition, the characteristic quadruple peaks of the DMPO–•OH adducts were also detected, but the peak intensity was extremely low (Fig. 12B), compared with the intensity of DMPO–•O_2^- adducts. This can be rationalized by considering the extremely short life-span of •OH, leading to the prompt quenching and combination to contribute the production of H_2O_2, since it has been demonstrated by scavenging study that •OH alone does not have any significant influence on the inactivation efficiency, probably due to the prevailing reactive species in the $CdIn_2S_4$ system is H_2O_2 instead of •OH. The strong intensity of DMPO–•O_2^- adducts guarantee the high production of •O_2^-, which is believed to be an important origin of H_2O_2 production in photocatalytic system, resulting in the $CdIn_2S_4$ microsphere to be a valuable VLD photocatalyst especially for H_2O_2-oriented photocatalytic oxidation process.

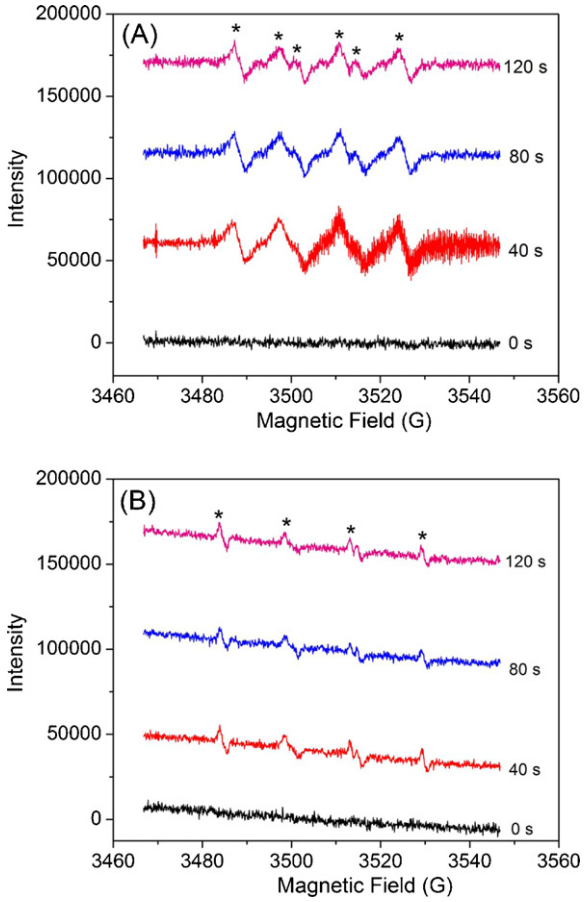

Fig. 12. DMPO spin-trapping ESR spectra recorded at ambient temperature in $CdIn_2S_4$ suspension under VL irradiation. (A) For DMPO–•O_2^- in methanol dispersion, and (B) for DMPO–•OH in aqueous dispersion.

4. Conclusions

In summary, we have applied a simple, facile and scalable process using ultrasonic spray pyrolysis to generate submicrometer sized $CdIn_2S_4$ spheres with microstructure without adding any template. The resulting products can be generated continuously at a rate of several grams per hour and no complex multi-step processes are required compared to other approaches. It was firstly found that $CdIn_2S_4$ can photocatalytically inactivate *E. coli* K-12 under VL irradiation without any doping or adding VLD photo-sensitizer. The bacterial inactivation by $CdIn_2S_4$ microspheres did not require direct contact with the photocatalyst, because large amounts of photon-generated H_2O_2 could diffuse into the bulk solution and cause damage to the bacterial cells. The detected concentration of H_2O_2 far exceeded the concentration in TiO_2-based photocatalyst systems. The destruction process of bacterial cell was from cell wall and cell membrane to other intracellular components. All these indicate that the $CdIn_2S_4$ microsphere, easily prepared by USP method in large-scale, is a true, stable and highly efficient VLD photocatalyst for bacterial inactivation, even without direct contact with the photocatalyst. This work not only provides a highly efficient VLD photocatalyst for H_2O_2-oriented photocatalytic reactions thus enlarging the family of VLD photocatalyst for low-cost water disinfection, but also creates avenues for the development of advanced photocatalytic disinfection reactors with partition system for facile photocatalyst separation and recycling. Any photocatalyst that can produce enough amounts of H_2O_2 under light irradiation can work in partition system for the indirect photocatalytic disinfection if the treated microorganisms are sensitive to H_2O_2 attacking.

Acknowledgments

The project was supported by a research grant (GRF 476811) from the Research Grant Council, Hong Kong SAR Government to P.K. Wong, and NSFC (21077104) to G.Y. Li and T.C. An.

Appendix A. Supplementary data

Supplementary data associated with this article can be found, in the online version, at http://dx.doi.org/10.1016/j.apcatb.2012.09.054.

References

[1] T. Matsunaga, R. Tomoda, T. Nakajima, H. Wake, FEMS Microbiology Letters 29 (1985) 211–214.
[2] A.K. Benabbou, Z. Derriche, C. Felix, P. Lejeune, C. Guillard, Applied Catalysis B: Environmental 76 (2007) 257–263.

[3] O.K. Dalrymple, E. Stefanakos, M.A. Trotz, D.Y. Goswami, Applied Catalysis B: Environmental 98 (2010) 27–38.
[4] P.C. Maness, S.L. Smolinski, D.M. Blake, Z. Huang, E.J. Wolfrum, W.A. Jacoby, Applied and Environmental Microbiology 65 (1999) 4094–4098.
[5] D.M. Blake, P.C. Maness, Z. Huang, E.J. Wolfrum, J. Huang, W.A. Jacoby, Separation and Purification Methods 28 (1999) 1–50.
[6] J.C. Yu, W. Ho, J. Yu, H. Yip, P.K. Wong, J. Zhao, Environmental Science and Technology 39 (2005) 1175–1179.
[7] K.S. Yao, D.Y. Wang, J.J. Yan, L.Y. Yang, W.S. Chen, Surface and Coatings Technology 201 (2007) 6882–6885.
[8] Y. Lan, C. Hu, X. Hu, J. Qu, Applied Catalysis B: Environmental 73 (2007) 354–360.
[9] C. Hu, Y. Lan, J. Qu, X. Hu, A. Wang, Journal of Physical Chemistry B 110 (2006) 4066–4072.
[10] H. Yu, X. Quan, Y. Zhang, N. Ma, S. Chen, H. Zhao, Langmuir 24 (2008) 7599–7604.
[11] W.J. Wang, Y. Yu, T.C. An, G.Y. Li, H.Y. Yip, J.C. Yu, P.K. Wong, Environmental Science and Technology 46 (2012) 4599–4606.
[12] B.B. Kale, J.O. Baeg, S.M. Lee, H. Chang, S.J. Moon, C.W. Lee, Advanced Functional Materials 16 (2006) 1349–1354.
[13] S.K. Apte, S.N. Garaje, R.D. Bolade, J.D. Ambekar, M.V. Kulkarni, S.D. Naik, S.W. Gosavi, J.O. Baeg, B.B. Kale, Journal of Materials Chemistry 20 (2010) 6095–6102.
[14] H. Nakanish, Japan Journal of Applied Physics 19 (1980) 103–108.
[15] S.N. Baek, T.S. Jeong, C.J. Youn, K.J. Hong, J.S. Park, D.C. Shin, Y.T. Yoo, Journal of Crystal Growth 262 (2004) 259–264.
[16] Y.C. Kang, I.W. Lenggoro, S.B. Park, K. Okuyama, Material Research Bulletin 35 (2000) 789–798.
[17] K. Okuyama, I.W. Lenggoro, N. Tagami, S. Tamaki, N. Tohge, Journal of Materials Science 32 (1997) 1229–1237.
[18] S.E. Skrabalak, K.S. Suslick, Journal of American Chemical Society 127 (2005) 9990–9991.
[19] J. Huang, W. Cheuk, Y. Wu, F.S.C. Lee, W. Ho, Catalysis Science and Technology 2 (2012) 1825–1827.
[20] L.S. Zhang, K.H. Wong, D.Q. Zhang, C. Hu, J.C. Yu, C.Y. Chan, P.K. Wong, Environmental Science and Technology 43 (2009) 7883–7888.
[21] M. Cho, H. Chung, W. Choi, J. Yoon, Applied and Environmental Microbiology 71 (2005) 270–275.
[22] W.J. Wang, L.Z. Zhang, T.C. An, G.Y. Li, H.Y. Yip, P.K. Wong, Applied Catalysis B: Environmental 108–109 (2011) 108–116.
[23] Y.M. Chen, A.H. Lu, Y. Li, L.S. Zhang, H.Y. Yip, H.J. Zhao, T.C. An, P.K. Wong, Environmental Science and Technology 45 (2011) 5689–5695.
[24] H. Bader, V. Sturzenegger, J. Hoigné, Water Research 22 (1988) 1109–1115.
[25] W.J. Wang, J.H. Bi, L. Wu, Z.H. Li, X.X. Wang, X.Z. Fu, Nanotechnology 50 (2008) 505705.
[26] K. Manickathai, S.K. Viswanathan, M. Alagar, Indian Journal of Pure and Applied Physics 46 (2008) 561–564.
[27] S.Y. Lee, K.J. Hong, Journal of the Korean Physical Society 50 (2007) 1789–1793.
[28] Y. Huang, W. Ho, Z. Ai, X. Song, L. Zhang, S. Lee, Applied Catalysis B: Environmental 89 (2009) 398–405.
[29] K.S.W. Sing, D.H. Everett, R.A.W. Haul, L. Moscou, R.A. Pierotti, J. Rouquerol, T. Siemieniewska, Pure and Applied Chemistry 57 (1985) 603–619.
[30] H.B. Fu, C.S. Pan, L.W. Zhang, Y.F. Zhu, Material Research Bulletin 42 (2007) 696–706.
[31] F. Dong, S.C. Lee, Z. Wu, Y. Huang, M. Fu, W.K. Ho, S. Zou, B. Wang, Journal of Hazardous Materials 195 (2011) 346–354.
[32] G.S. Li, D.Q. Zhang, J.C. Yu, M.H. Leung, Environmental Science and Technology 44 (2010) 4276–4281.
[33] J.W. Tang, Z.G. Zou, J.H. Ye, Chemistry of Materials 16 (2004) 1644–1649.
[34] J.C. Yu, X.C. Wang, X.Z. Fu, Chemistry of Materials 16 (2004) 1523–1530.
[35] H.X. Li, Z.F. Bian, J. Zhu, D.Q. Zhang, G.S. Li, Y.N. Huo, H. Li, Y.F. Lu, Journal of American Chemical Society 129 (2007) 8406–8407.
[36] K.Y. Jung, S.B. Park, Applied Catalysis B: Environmental 25 (2000) 249–256.
[37] A.G. Rincón, C. Pulgarin, Applied Catalysis B: Environmental 49 (2004) 99–112.
[38] R. Jin, W. Gao, J. Chen, H. Zeng, F. Zhang, Z. Liu, N. Guan, Journal of Photochemistry and Photobiology A: Chemistry 162 (2004) 585–590.
[39] L.S. Zhang, K.H. Wong, H.Y. Yip, C. Hu, J.C. Yu, C.Y. Chan, P.K. Wong, Environmental Science and Technology 44 (2010) 1392–1398.
[40] Y.X. Chen, S.Y. Yang, K. Wang, L.P. Lou, Journal of Photochemistry and Photobiology A: Chemistry 172 (2005) 47–54.
[41] A.A. Khodja, A. Boulkamh, C. Richard, Applied Catalysis B: Environmental 59 (2005) 147–154.
[42] S.G. Schrank, H.J. José, R.F.P.M. Moreira, Journal of Photochemistry and Photobiology A: Chemistry 147 (2002) 71–76.
[43] D. Lejeune, M. Hasanuzzaman, A. Pitcock, J. Francis, I. Sehgal, Molecular Cancer 5 (2006) 21.
[44] M. Cho, H. Chung, W. Choi, J. Yoon, Water Research 38 (2004) 1069–1077.
[45] K.T. Ranjit, I. Willner, S.H. Bossmann, A.M. Braun, Environmental Science and Technology 35 (2001) 1544–1549.
[46] K.T. Ranjit, H. Cohen, I. Willner, S. Bossmann, A.M. Braun, Journal of Materials Science 34 (1999) 5273–5280.
[47] Z. Zhang, X. Wang, J. Long, Z. Ding, X. Fu, X. Fu, Applied Catalysis A: General 380 (2010) 178–184.
[48] F. Shiraishi, C. Kawanishi, Journal of Physical Chemistry A 108 (2004) 10491–10496.
[49] Y. Kikuchi, K. Sunada, T. Iyoda, K. Hashimoto, A. Fujishima, Journal of Photochemistry and Photobiology A: Chemistry 106 (1997) 51–56.
[50] J. Yu, J. Chen, C. Li, X. Wang, B. Zhang, H. Ding, Journal of Physical Chemistry B 108 (2004) 2781–2783.
[51] R.F. Howe, M. Grätzel, Journal of Physical Chemistry 89 (1985) 4495–4499.
[52] J. Ren, W.Z. Wang, L. Zhang, J. Chang, S. Hu, Catalysis Communications 10 (2009) 1940–1943.